



HERCULES-2 Project

Fuel Flexible, Near Zero Emissions, Adaptive Performance Marine Engine

Deliverable: **D4.4**

TMF model for new cylinder head

<Final>

Nature of the Deliverable: Report
Due date of the Deliverable: 28 February 2018
Actual Submission Date: 06 March 2018
Dissemination Level: Public

Contributors: Offenburg University of Applied Sciences
Andreas Jilg, MSc. and Professor Dr.-Ing. Thomas Seifert

Work Package Leader Responsible: Dr. R. Thumser (MDT-AUG)



Start date of Project: 01/05/2015 Duration: 42 months

Grant Agreement No: **634135-HERCULES-2**

HORIZON 2020
The EU Framework Programme for Research and Innovation



TABLE OF CONTENTS

1	Executive Summary	3
2	Introduction	3
3	Objectives	3
4	Description of Activities	4
4.1	Plasticity models.....	4
4.1.1	Advanced time and temperature dependent plasticity model	4
4.1.2	Simplified plasticity models.....	5
4.1.3	Determination and validation of the material properties	6
4.2	Multiaxial TMF life prediction models	13
4.2.1	Simple life prediction model.....	13
4.2.2	Mechanism-based D_{TMF} life prediction model.....	14
4.3	Comparison of models based on finite-element calculations.....	14
5	Conclusions	16
6	References.....	17

1 Executive Summary

Thermodynamic concepts of exhaust gas treatment, reduction of specific fuel oil or intensified usage of exhaust gas energy go along with higher component temperatures and mechanical loads. To be able to find an appropriate material that sustains the higher loads throughout the intended lifetime and a material-specific design of the component, numerical simulations of the thermomechanical fatigue behaviour of components are necessary. This requires on the one hand reliable material models that can describe the time and temperature dependent plasticity and damage of the material. On the other hand, however, computation times should be practical so that iterative design optimizations via finite-element calculations are possible.

This report summarizes the activities within WP4.1 “New materials and design for cylinder heads”, and more precisely the results of numerical studies on material modelling, where advanced and simplified plasticity models are compared with respect to multiaxial TMF life predictions. The results of the studies show that for the considered TMF loadings even simplified models can be applied for fatigue life prediction without a significant loss of accuracy in the prediction.

2 Introduction

Increasing the efficiency of internal combustion engines is directly related to increasing specific power and, thus, increasing combustion pressure and temperature. One key component of the engine is the cylinder head, which must withstand these higher temperatures and higher pressures. Hence, computational methods are required for the assessment of the fatigue life of the cylinder head comprising models for the description of the time and temperature dependent plasticity and damage in finite-element calculations.

3 Objectives

In this work package, at Offenburg University of Applied Science on the one hand an advanced plasticity model is considered and on the other hand simplified plasticity models are assessed with respect to their predictive capability compared to the advanced models. For thermomechanical fatigue (TMF) life prediction also a simple model as well as the advanced mechanism-based D_{TMF} model is considered. For the determination of the corresponding material properties of the models experimental results of tensile tests, complex low-cycle fatigue (CLCF, different strain rates, stress relaxation phases) and TMF tests provided by Fraunhofer Institute for Mechanics of Materials IWM in this work package are used. The loading history in the CLCF tests consists of different strain rates and hold times in tension and compression as well as different strain amplitudes. With this complex loading program strain rate effects, stress relaxation and the cyclic hardening properties of the material can be investigated in a single experiment and sufficient information is generated for the determination of the parameters of the plasticity model.

4 Description of Activities

4.1 Plasticity models

A good description of the stresses and (plastic) strains in finite-element calculations of components is a key aspect of a predictive TMF life model. Hence, an advanced time and temperature dependent plasticity model is established for application in finite-element calculations that can describe the response of the considered cast iron material under thermomechanical loading conditions. However, advanced plasticity models contain a relative large number of material properties and, thus, special material tests that are often not available are necessary to reasonably determine the properties. Moreover, the computational cost in using advanced plasticity models in finite-element calculations is generally higher than using simplified plasticity models. Hence, simplified plasticity models are applied to assess the relevance of different model features (e.g. viscosity and hardening). On the basis of experimental data (complex LCF, TMF) of the considered cast iron materials, the material properties of an advanced plasticity model and the simplified models are determined based on the CLCF tests and validated based on the TMF tests. In section 4.1.1 and 4.1.2 the used plasticity models are described, before in section 4.1.3 the determination of the corresponding material properties is addressed.

4.1.1 Advanced time and temperature dependent plasticity model

Advanced plasticity models exist that can describe the time and temperature dependent cyclic material behaviour. The Bauschinger effect can be taken into account with kinematic hardening, so that realistic stress-strain hysteresis loops are obtained with the models [1][2]. The time dependent material behaviour is accounted for with viscoplastic models. A well-known viscoplastic model is the Chaboche model with its manifold versions [3]. In this work, a version of the Chaboche model was used successfully to describe the plasticity of high temperature materials, e.g. [4][5][6][7].

The stresses σ_{ij} are computed from the strains ε_{ij} via

$$\sigma_{ij} = C_{ijkl} (\varepsilon_{kl} - \varepsilon_{kl}^{th} - \varepsilon_{kl}^{vp}) \quad (1)$$

where C_{ijkl} is the elasticity tensor. The thermal strains are given by the expansion coefficient α_{th} and the difference in temperature with respect to an initial temperature ΔT :

$$\varepsilon_{ij}^{th} = \alpha^{th} \Delta T \delta_{ij} \quad (2)$$

δ_{ij} is the second order identity tensor. The viscoplastic strain rate

$$\dot{\varepsilon}_{ij}^{vp} = \frac{3}{2} \dot{p} \frac{\beta_{ij}}{\beta_{eq}} \quad (3)$$

is described with the power law for the equivalent viscoplastic strain rate

$$\dot{p} = \left\langle \frac{\beta_{eq} - R_e}{K} \right\rangle^n \quad (4)$$

$\beta_{ij} = \sigma'_{ij} - \alpha_{ij}$ is the relative stress where σ'_{ij} denotes the deviator of the stress tensor and α_{ij} is the backstress tensor. β_{eq} is the von Mises equivalent stress value. The backstress tensor is the sum of two parts each following the evolution equation ($k = 1, 2$)

$$\dot{\alpha}_{ij}^{(k)} = C^{(k)} \dot{\varepsilon}_{ij}^{vp} - \gamma^{(k)} \varphi^{(k)} \dot{p} \alpha_{ij}^{(k)} - R^{(k)} \alpha_{ij}^{(k)} + \frac{\partial C^{(k)}}{\partial T} \frac{1}{C^{(k)}} \dot{T} \alpha_{ij}^{(k)} \quad (5)$$

The functions

$$\varphi^{(k)} = \varphi_{ss}^{(k)} + \left(1 - \varphi_{ss}^{(k)}\right) e^{-\omega^{(k)} p} \quad (6)$$

are introduced to model kinematic cyclic hardening or softening. Further, the model contains the temperature dependent material properties:

- E and α_{th} , describing the thermoelastic properties of the material
- K and n , describing the viscous properties of the material
- R_e , $C^{(k)}$, $\gamma^{(k)}$, $R^{(k)}$, $\varphi_{ss}^{(k)}$ and $\omega^{(k)}$, describing the plastic and hardening properties of the material

4.1.2 Simplified plasticity models

Four stages of simplification of the advanced time and temperature dependent plasticity model are considered. The first simplification does not consider kinematic cyclic hardening or softening. Hence $\varphi_{ss}^{(k)} = 1$ in equation (6). This simplified model is available in the finite-element program ANSYS. The second simplified model neglects static recovery of kinematic hardening. Hence, $R^{(k)} = 0$ in equation (5). This simplified kinematic hardening law is available in the finite-element program ABAQUS using the option `*PLASTIC, HARDENING=COMBINED` and can be used in combination with the power law for the equivalent viscoplastic strain rate selected by the ABAQUS option `*RATE DEPENDENT`

$$\dot{p} = D \left\langle \frac{\beta_{eq}}{R_e} - 1 \right\rangle^n \quad (7)$$

This plasticity model, which is still a time and temperature dependent model, thus, contains the following material properties:

- E and α_{th} , describing the thermoelastic properties of the material
- D and n , describing the viscous properties of the material
- R_e , $C^{(k)}$ and $\gamma^{(k)}$ describing the plastic and hardening properties of the material

In the third simplification, the time dependent material behaviour is additionally neglected compared to the previous simplification. The equivalent plastic strain rate is therefore not explicitly defined as it is the case for the equivalent viscoplastic strain rate defined by equation (4) and (7). It

is implicitly determined by the consistency condition that states that in case of plastic yielding the yield surface defined by the von Mises yield function

$$\phi = \beta_{eq} - R_e \quad (8)$$

cannot be exceeded:

$$\dot{\phi} = 0 \quad (9)$$

The third simplified plasticity model, which is now a rate-independent model, contains the following material properties:

- E and α_{th} , describing the thermoelastic properties of the material
- R_e , $C^{(k)}$ and $\gamma^{(k)}$ describing the plastic and hardening properties of the material

The fourth simplified model differs from the previous one by the use of only one backstress.

4.1.3 Determination and validation of the material properties

For determination and validation of the material properties, the plasticity models are implemented for uniaxial stress states. The determination of the properties is based on a combined experience-based and numerical optimization based approach. A gradient-based algorithm is implemented and used. The material properties are determined for each test temperature individually. For TMF conditions, the properties are linearly interpolated in temperature.

In a first step, the temperature dependent material properties of the rate-independent plasticity model (fourth simplified model) are determined for cast iron “material F” based on tensile tests. The experimental stress-strain curves and the stress-strain curves computed with the model are shown for the respective test temperatures in Figure 2. The material properties determined from the tensile tests are used to predict the stresses of a TMF test with the temperature range from 50 to 500 °C (Figure 3). The model prediction of the TMF test is appropriate for the considered simple plasticity model.

In the second step, the temperature dependent material properties of the advanced model as well as of the simplified models for the cast iron material F and of the advanced model as well as of the second simplified model for the cast iron “material D” are determined. For this, the determined material properties of the advanced model are stepwise adapted to describe the experimental data with the simplified models (see Table 1). To this end, CLCF tests at room temperature, 300, 350, 400, 450 and 500 °C are used. An exemplary complex strain history of a CLCF test with the different strain rates and hold times in tension and compression is shown in Figure 1. Measured and with the second simplified model (no. 2) calculated stress histories and the corresponding stress-strain curves are shown exemplarily for room temperature, 350 and 500 °C in Figure 4 for material F and in Figure 6 for material D. Additionally, measured and with the fourth simplified model calculated stress histories and the corresponding stress-strain curves are shown for room

temperature, 350 and 500 °C for material F in Figure 5. The determined material properties are used to predict the stresses of six different TMF tests for both materials. In Figure 7, Figure 8 and Figure 9 measured and calculated stress histories and the corresponding stress-strain curves are shown for an exemplarily TMF test with the temperature range from 50 to 500 °C.

no	model	material properties	adaption of	adaption to
1	advanced model	$E, \alpha_{th}, R_e, C^{(k)}, \gamma^{(k)}, K, n, R^{(k)}, \varphi_{ss}^{(k)}, \omega^{(k)}$	all values	
2	first simplified	$E, \alpha_{th}, R_e, C^{(k)}, \gamma^{(k)}, K, n, R^{(k)}$	R_e	
3	model		$C^{(k)}$	
4	second simplified	$E, \alpha_{th}, R_e, C^{(k)}, \gamma^{(k)}, K, n$	R_e, K	
5	model	$E, \alpha_{th}, R_e, C^{(k)}, \gamma^{(k)}, D$		
6	third simplified	$E, \alpha_{th}, R_e, C^{(k)}, \gamma^{(k)}$	$R_e, C^{(k)}, \gamma^{(k)}$	high
7	model			low
8	fourth simplified	$E, \alpha_{th}, R_e, C, \gamma$	R_e, C, γ	high
9	model			low

Table 1: Determined material properties and their adaption of the investigated models

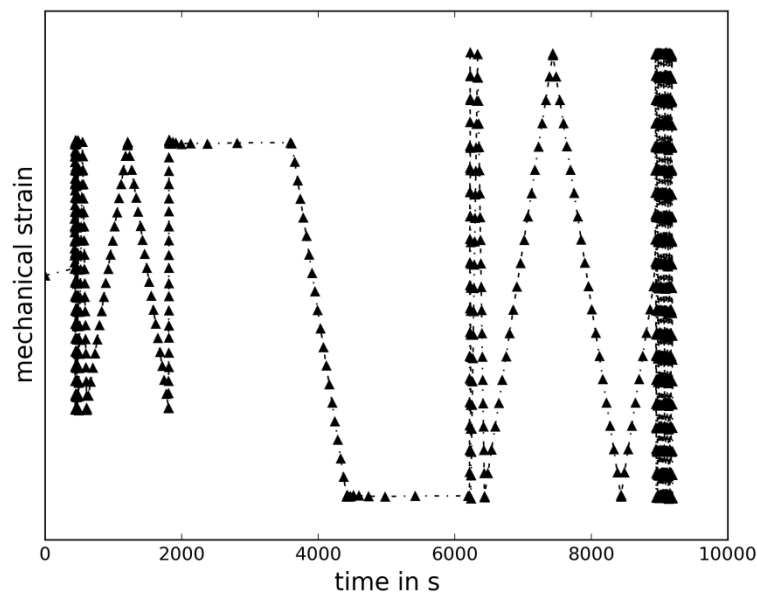


Figure 1: Exemplary complex strain history of a CLCF experiment

The CLCF stress-time curves show a notable better description using the advanced model. Especially during the dwell times, the second simplified model is not suitable due to the missing static recovery term in the kinematic hardening law. However, the models show less deviation at the TMF experiments.

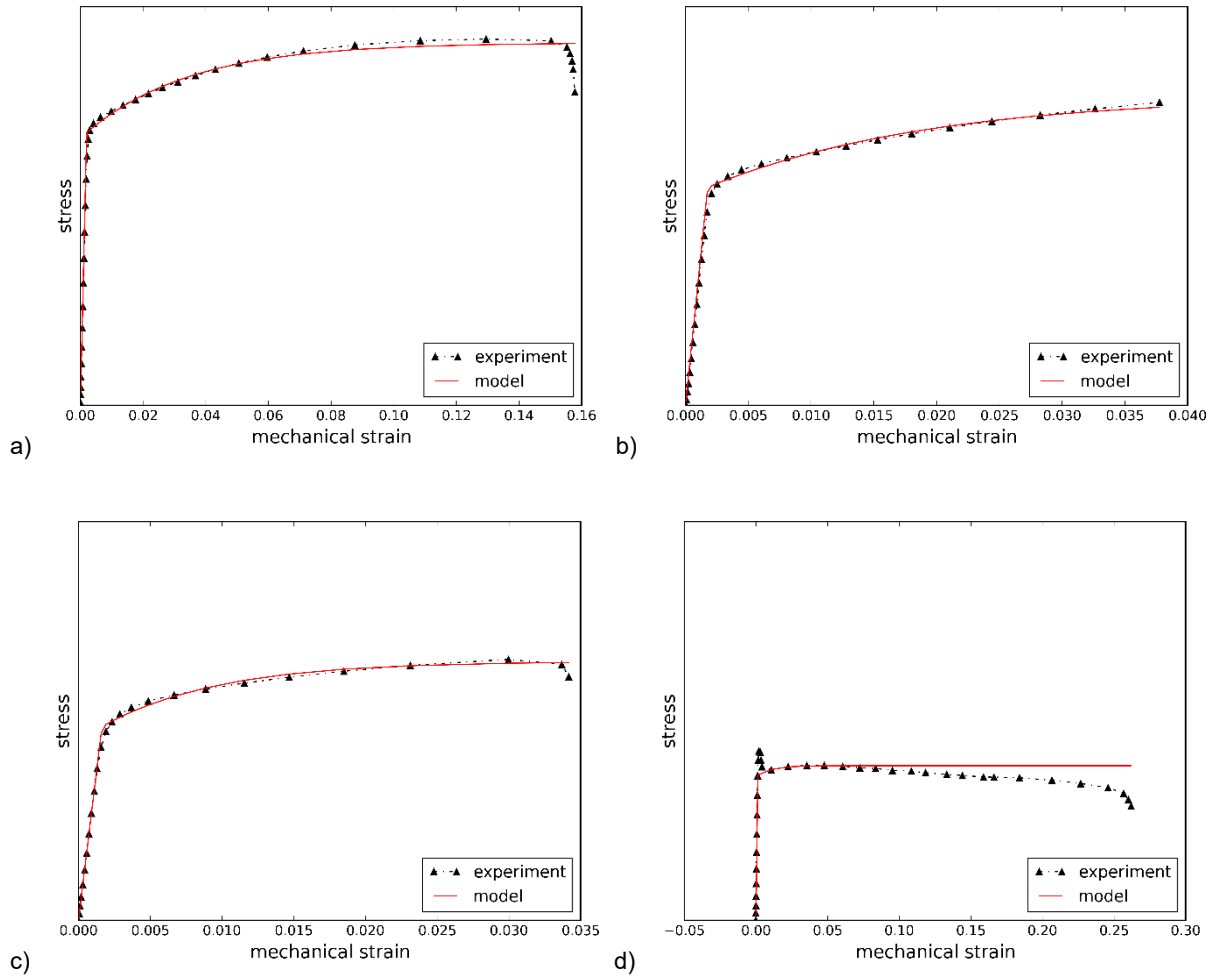


Figure 2: Experimental results of tensile tests and model response computed with determined material properties for material F: a) room temperature; b) 300 °C; c) 400 °C; d) 500 °C (same scale is used in all figures)

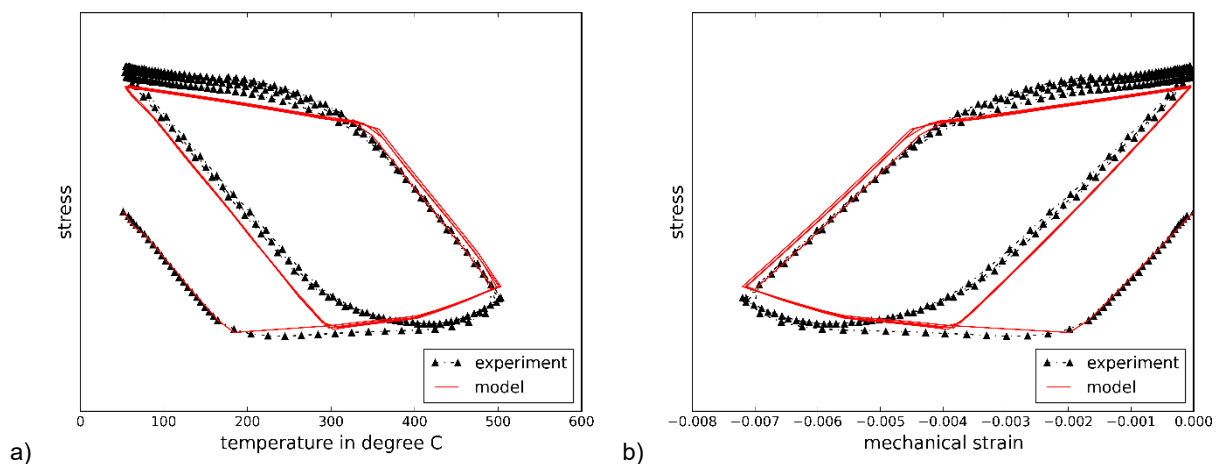


Figure 3: Experimental results of a TMF test with the temperature range from 50 to 500 °C and the model prediction for material F with the material properties determined on the basis of the tensile tests: a) stress-temperature hysteresis loops; b) stress-mechanical strain hysteresis loops (same scale is used as in Figure 2)

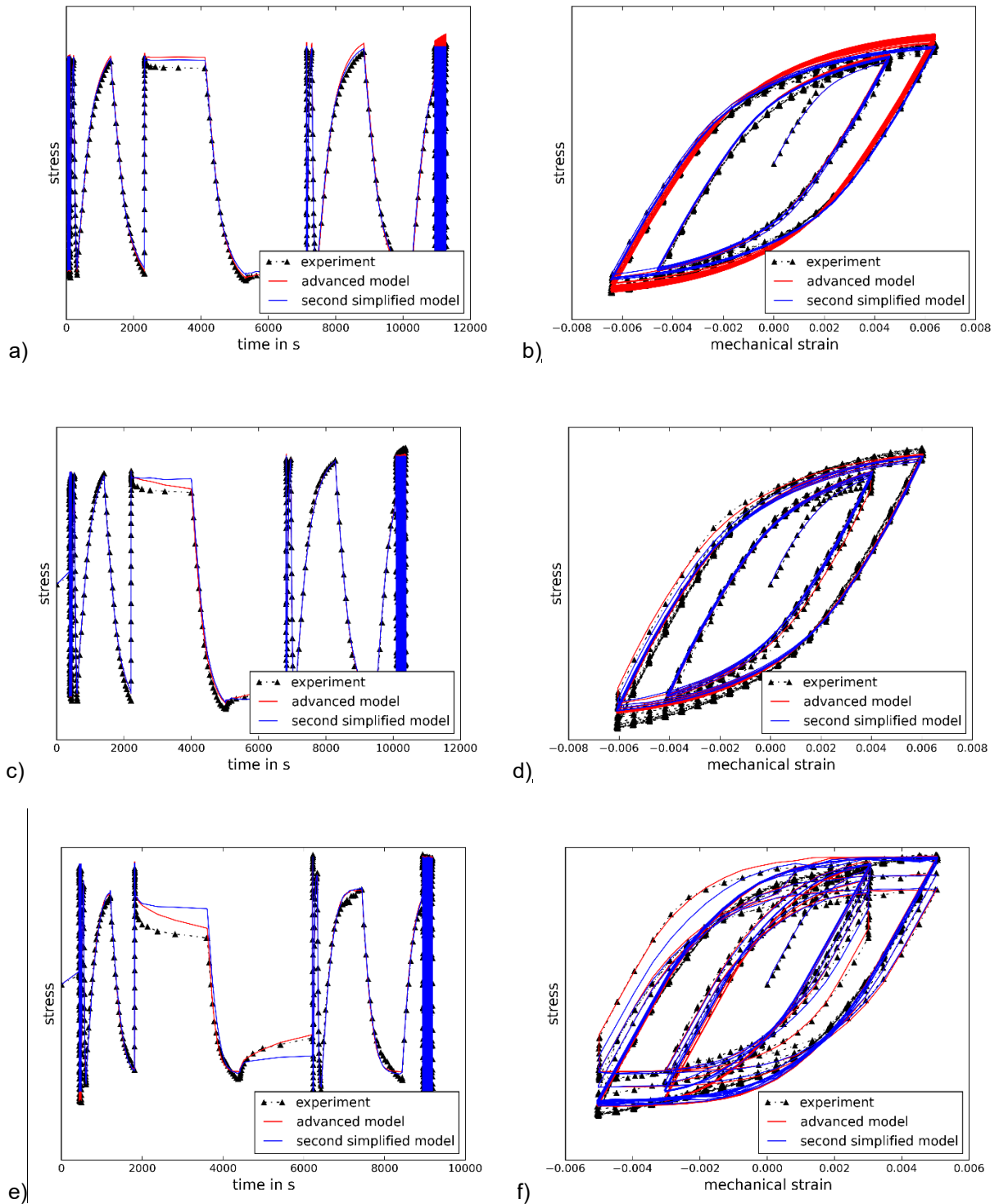


Figure 4: Experimental results of CLCF tests and model response of the advanced and of the second simplified model computed with determined material properties for material F: a) room temperature stress-time; b) room temperature stress-strain; c) 350 °C stress-time; d) 350 °C stress-strain; e) 500 °C stress-time; f) 500 °C stress-strain

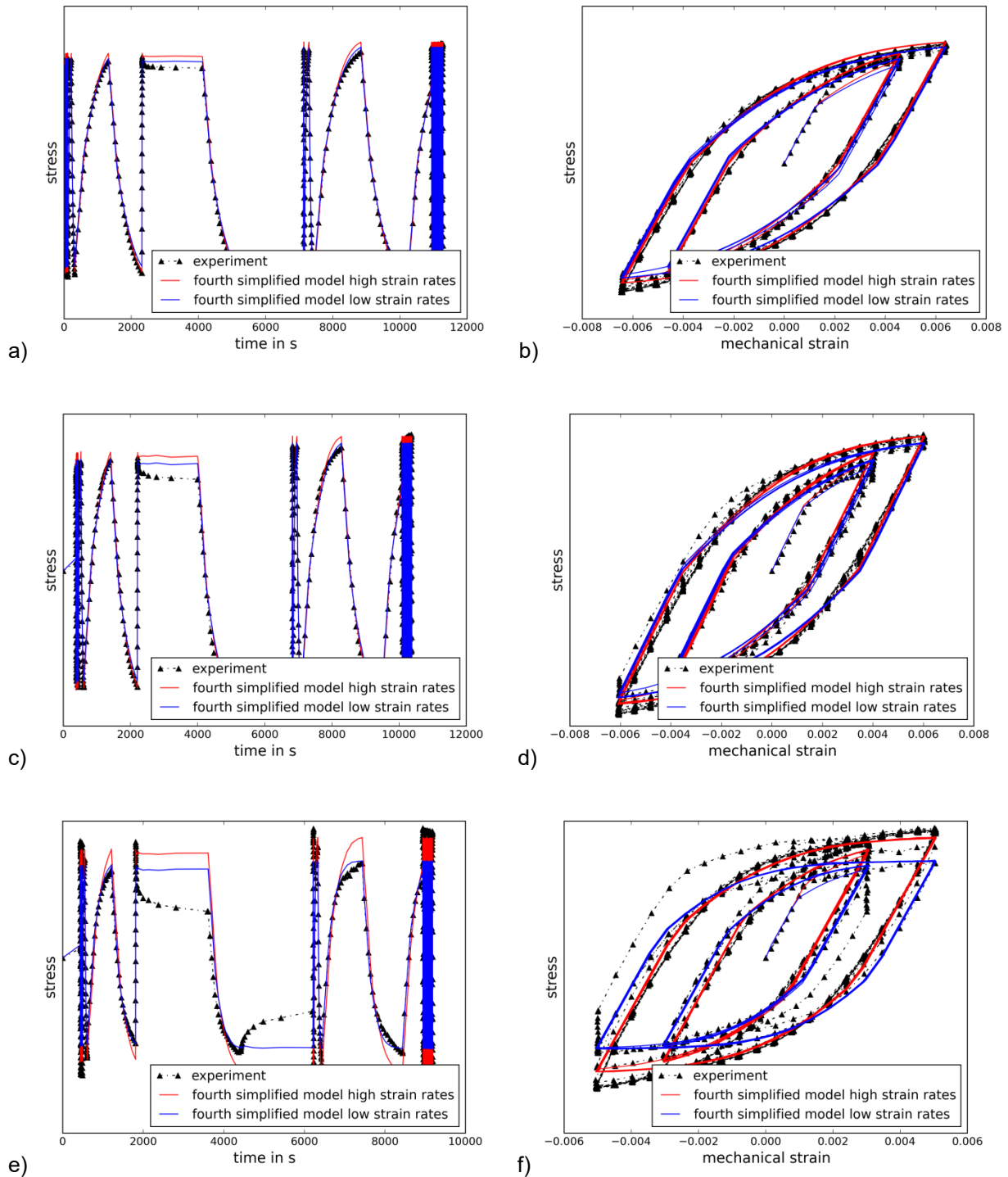


Figure 5: Experimental results of CLCF tests and model response of the fourth simplified model computed with determined material properties for material F: a) room temperature stress-time; b) room temperature stress-strain; c) 350 °C stress-time; d) 350 °C stress-strain; e) 500 °C stress-time; f) 500 °C stress-strain

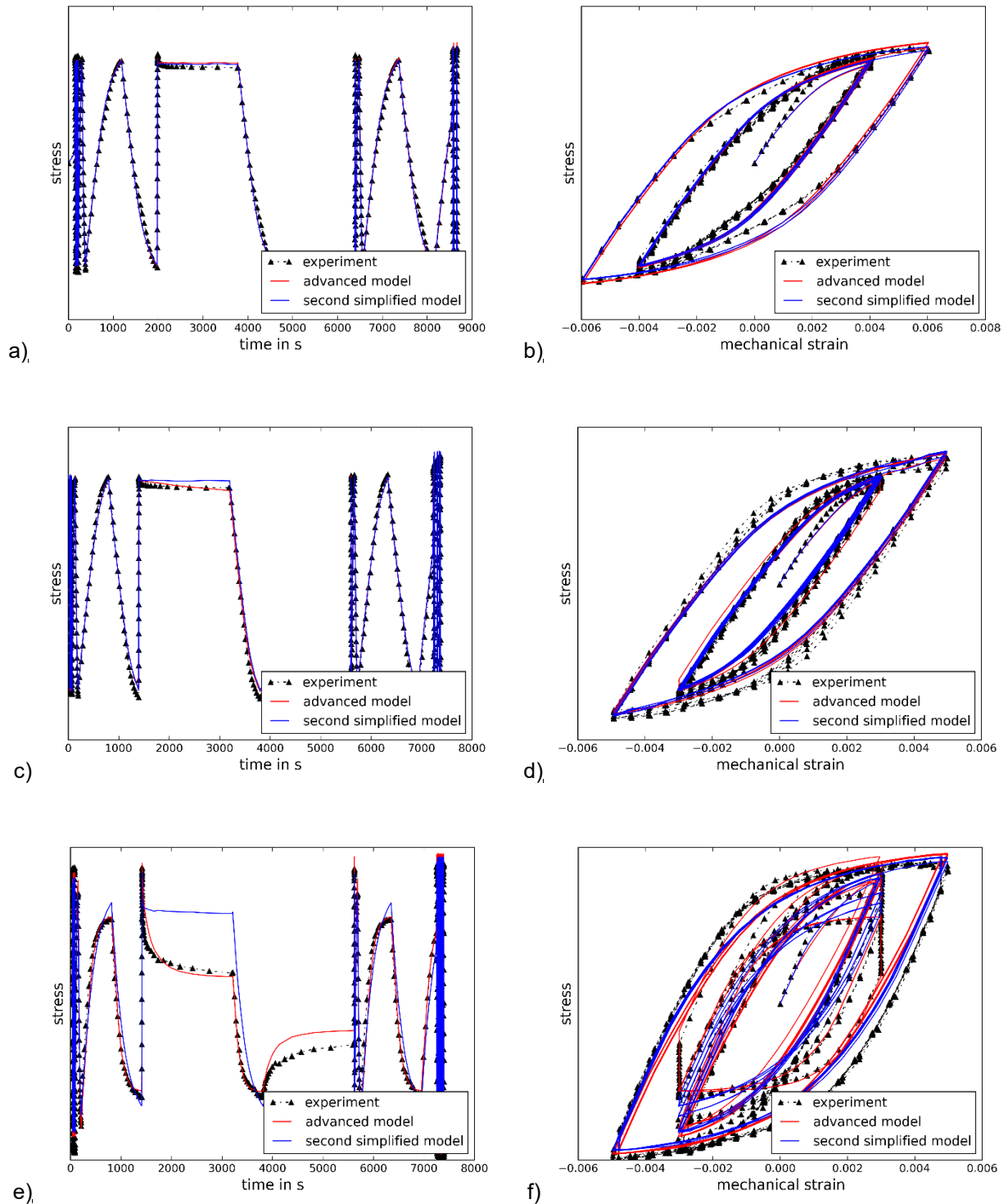


Figure 6: Experimental results of CLCF tests and model response of the advanced and of the second simplified model computed with determined material properties for material D: a) room temperature stress-time; b) room temperature stress-strain; c) 350 °C stress-time; d) 350 °C stress-strain; e) 500 °C stress-time; f) 500 °C stress-strain

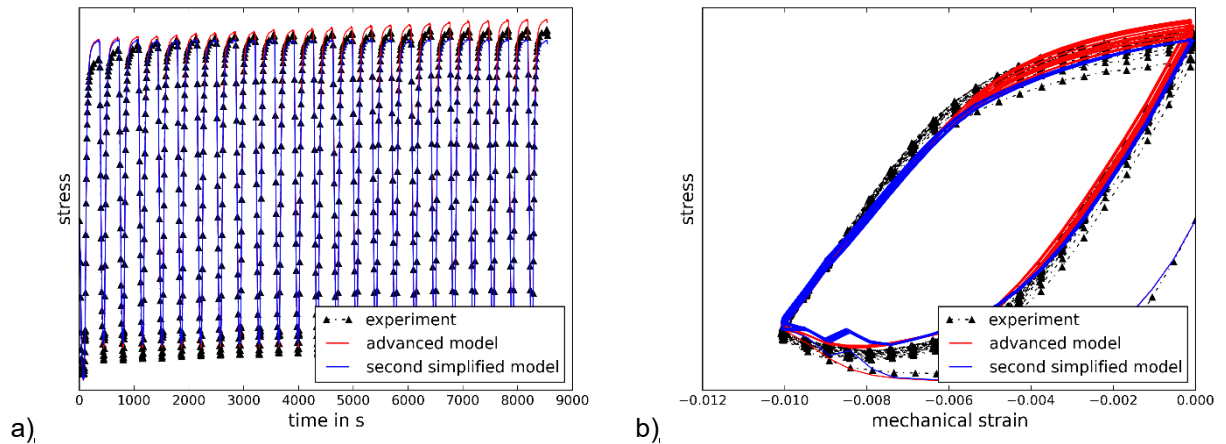


Figure 7: Experimental results of a TMF test with the temperature range from 50 to 500 °C and the model predictions of the advanced and of the second simplified model for material F with the material properties determined on the basis of the CLCF tests: a) stress-time curve; b) stress-mechanical strain hysteresis loops

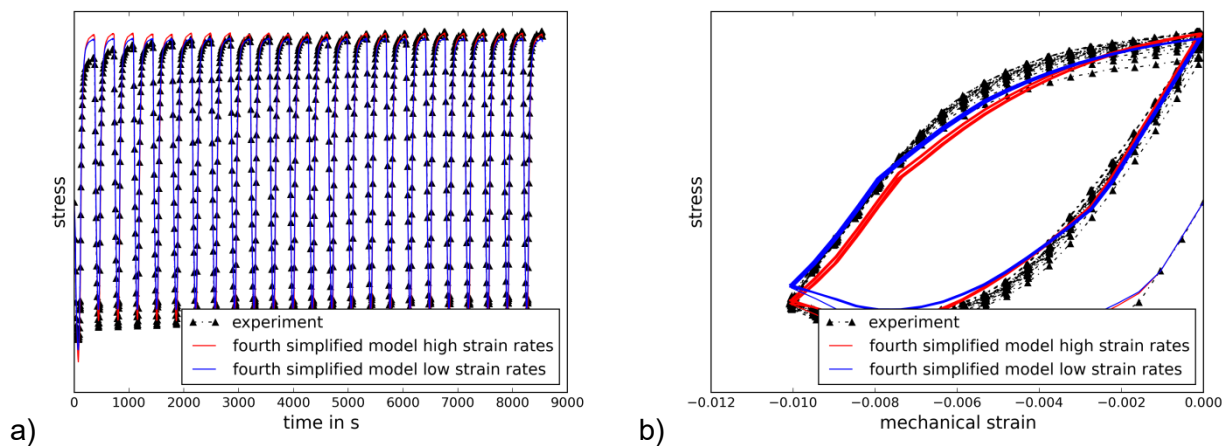


Figure 8: Experimental results of a TMF test with the temperature range from 50 to 500 °C and the model predictions of the second simplified model for material F with the material properties determined on the basis of the CLCF tests: a) stress-time curve; b) stress-mechanical strain hysteresis loops

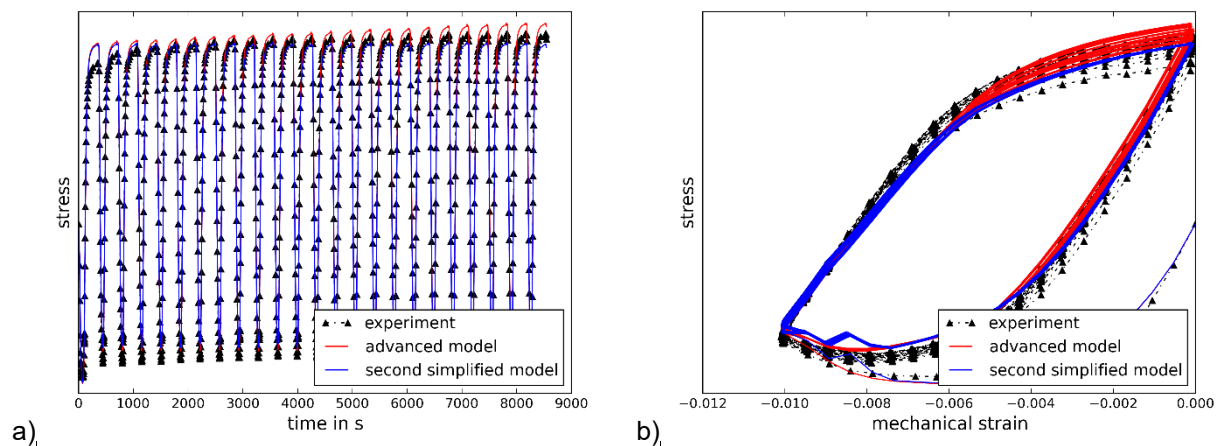


Figure 9: Experimental results of a TMF test with the temperature range from 50 to 500 °C and the model predictions of the advanced and of the second simplified model for material D with the material properties

determined on the basis of the CLCF tests: a) stress-time curve; b) stress-mechanical strain hysteresis loops

4.2 Multiaxial TMF life prediction models

For TMF-life prediction on the basis of stresses and (plastic) strains obtained in finite-element calculations, a model is necessary that accounts for multiaxial, proportional and non-proportional loading histories. To this end, a simple life prediction model is used that is based on strain-life curves as well as a mechanism-based life prediction model, that describes the time and temperature dependent fatigue crack growth and is known as D_{TMF} concept [4][5].

In section 4.2.1, the simple model for fatigue life prediction is shown with the corresponding properties and in section 4.2.2, the mechanism-based D_{TMF} model is briefly described.

4.2.1 Simple life prediction model

The simple life prediction model considers the maximum principal value of the mechanical strain range tensor as damage parameter that can be correlated to the number of cycles to failure:

$$N_f = A(\Delta\varepsilon_{L,max}^{mech})^{-B} \quad (10)$$

The subscript *max* indicates that the two time points of the loading history are identified in an optimization procedure that result in the maximal principal mechanical strain range and, hence, in the minimal fatigue life. The fatigue properties A and B are determined on results of TMF tests (see Figure 10).

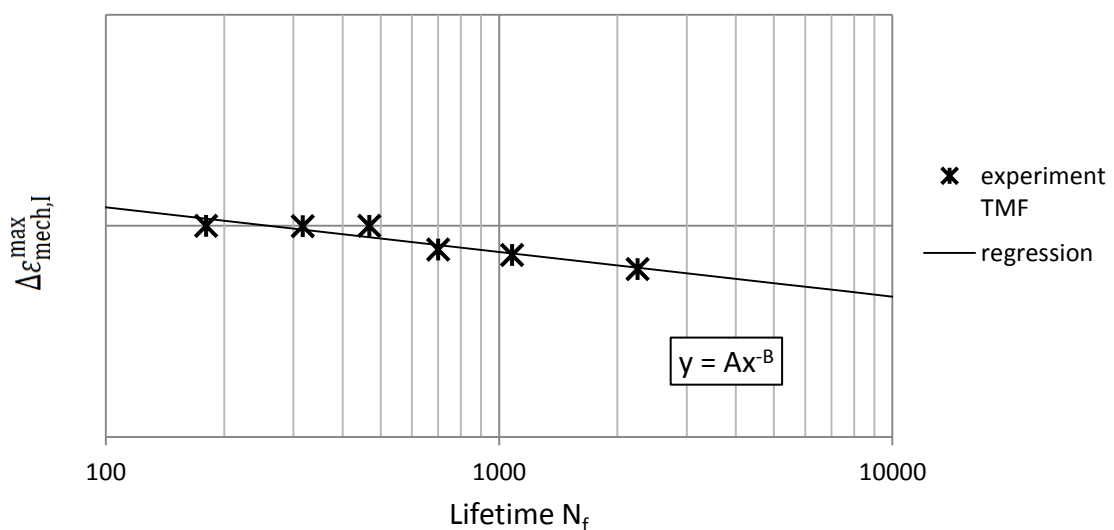


Figure 10: Wöhler curve of the TMF experiments for Material F

4.2.2 Mechanism-based D_{TMF} life prediction model

The mechanism-based D_{TMF} model is based on the crack-tip blunting model. It assumes that the increment in crack advance per loading cycle da/dN is correlated with the cyclic crack-tip opening displacement $\Delta CTOD$:

$$\frac{da}{dN} = \beta \Delta CTOD^B = \beta (d_n D_{TMF} a)^B \quad (11)$$

The analytical fracture mechanics based estimate $\Delta CTOD$ contains the damage parameter D_{TMF} , the factor d_n depending on the hardening exponent n' and the crack length a . The exponent B and the factor β are fatigue crack growth properties which are typically temperature independent. In the project a modified model is developed by Fraunhofer IWM that accounts for intergranular embrittlement (IE) and uses a temperature dependent factor β that is denoted as β_{IE} . By integration of the crack growth law from an initial crack length a_0 (assumed to be present from the beginning, since cracks initiate early for LCF and TMF) to a crack length at failure a_f , the explicit expression for the number of cycles to failure

$$N_f = \frac{a_f^{1-B} - a_0^{1-B}}{\beta_{IE}(1-B)} (d_n D_{TMF})^{-B} \quad (12)$$

is obtained.

4.3 Comparison of models based on finite-element calculations

The advanced time and temperature dependent plasticity model is implemented as user-defined subroutine UMAT in ABAQUS, so that it can be applied to calculate the stresses and (plastic) strains in a cylinder head specimen that is tested at Fraunhofer Institute for Chemical Technology ICT. To this end, an implicit numerical integration scheme is used [8][9]. The Fraunhofer ICT provided the temperature fields for the calculations. Three thermodynamic cycles are calculated and out of the last one, the lifetime is determined.

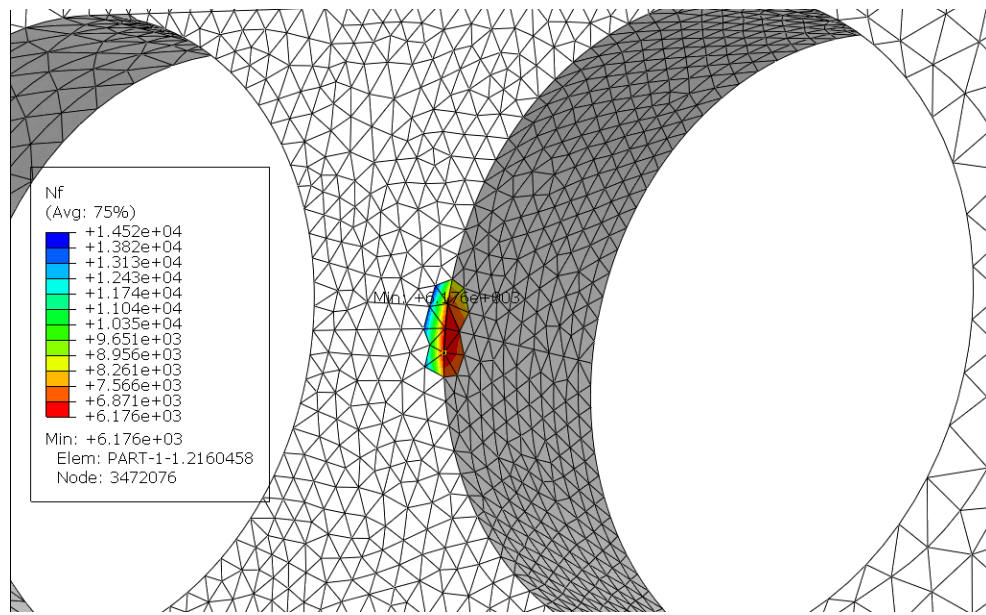


Figure 11: Finite-element model of the cylinder head specimen showing the number of cycles to failure N_f in the critical area of the advanced model for material F

The cylinder head specimen (see Figure 11) is used to compare the models regarding their prediction accuracy. The results are shown in Figure 12. The slope of the Wöhler curve is quite low. Thus, even small deviations of maximal principal mechanical strain range can lead to large deviations in the determined lifetime.

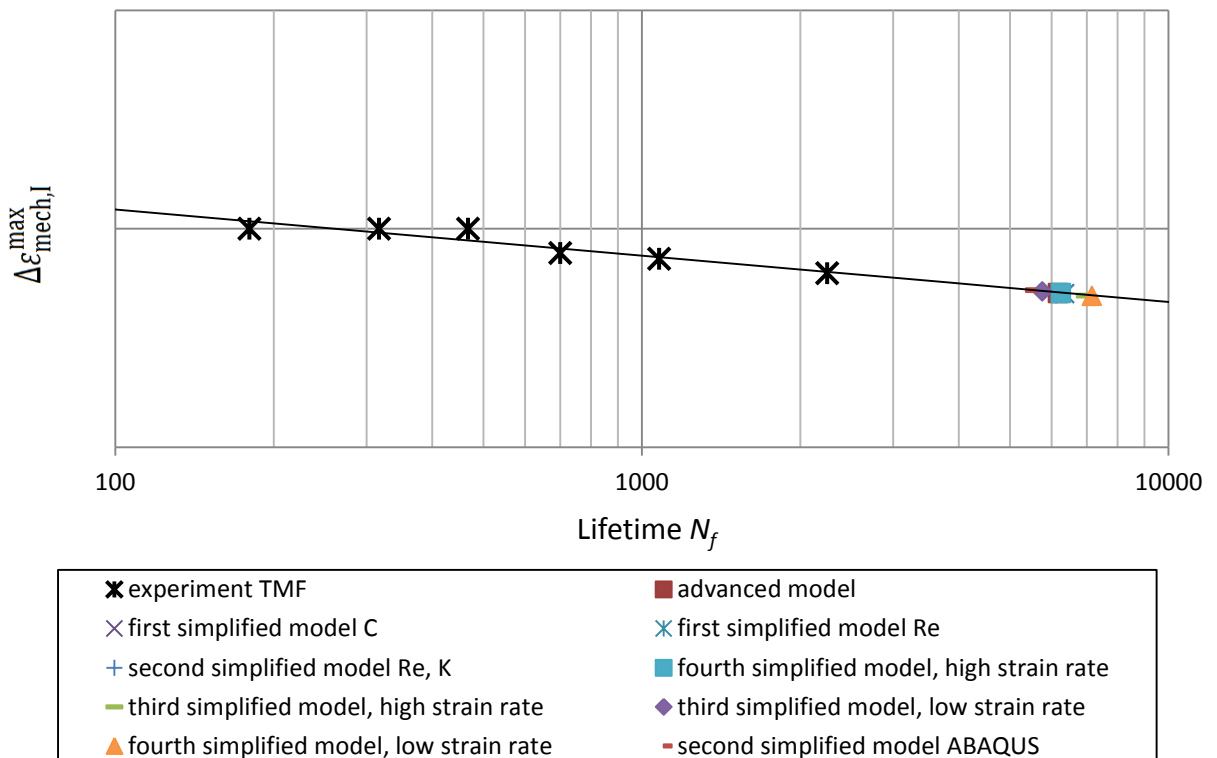


Figure 12: Wöhler curve with calculated lifetimes of the different models for material F

5 Conclusions

The material properties of the considered plasticity models with different level of complexity are determined based on isothermal CLCF tests at different temperatures. The results show that the deviation of the calculated and the experimentally measured stress response in the CLCF tests increases with decreasing complexity of the plasticity model. However, the deviation of the respective models when applied to the TMF tests is not significant and therefore less complex models could be suitable for lifetime evaluation. The scatter in the maximal principal mechanical strain range is below 3%. Hence, in practice, calculations can be done with the simplified models if the loading conditions are close to the conditions represented by the considered TMF tests.

6 References

- [1] P.J. Armstrong, C.O. Frederik, A mathematical representation of the multiaxial Bauschinger effect, Central Electricity Generating Board, Report RD/B/N 731, 1966
- [2] J.L. Chaboche, Time-independent constitutive theories for cyclic plasticity, *Int. J. Plast.* 2, 1986, 149-188
- [3] J.L. Chaboche, Constitutive equations for cyclic plasticity and cyclic viscoplasticity, *Int. J. Plast.* 5, 1989, 247-302
- [4] T. Seifert, H. Riedel, G. Pramhams, G. Bumberger, Novel lifetime models for high temperature components, *AutoTechnology* 7, 2007, 34-38
- [5] T. Seifert, H. Riedel, Fatigue Life Prediction of High Temperature Components in Combustion Engines and Exhaust Systems, in: *Proceedings of the 4th European Automotive Simulation Conference* (Eds. K.W. Seibert, M. Jirka), Ansys Inc, 2009, 313-324.
- [6] T. Seifert, C. Schweizer, M. Schlesinger, M. Möser, M. Eibl, Thermomechanical fatigue of 1.4849 cast steel – experiments and life prediction using a fracture mechanics approach, *International Journal of Materials Research* 101, 2010, 942-950
- [7] R.-K. Krishnasamy, T. Seifert, D. Siegele, A computational approach for thermomechanical fatigue life prediction of dissimilarly welded superheater tubes, in: *Materials for Advanced Power Engineering 2010* (Eds. J. Lecomte-Beckers, Q. Contrepois, T. Beck, B. Kuhn), 9th Liege Conference, 2010, 1126-1135
- [8] T. Seifert, T. Schenk, I. Schmidt, Efficient and modular algorithms in modeling finite inelastic deformations: objective integration, parameter identification and sub-stepping techniques, *Computer Methods in Applied Mechanics and Engineering* 196 (2007), 2269-2283
- [9] T. Seifert, I. Schmidt, Line-search methods in general return mapping algorithms with application to porous plasticity, *International Journal for Numerical Methods in Engineering* 73 (2008), 1468-1495